PNAS RESEARCH ARTICLE | EARTH, ATMOSPHERIC, AND PLANETARY SCIENCES OPEN ACCESS

Evidence of nitrate-based nighttime atmospheric nucleation driven by marine microorganisms in the South Pacific

Guillaume Chamba[a], Matti Rissanen[b,c], Theresa Barthelmeß[d], Alfonso Saiz-Lopez[e], Clémence Rose[a], Siddharth Iyer[b], Alexia Saint-Macary[f,g], Manon Rocco[a], Karl Safi[h], Stacy Deppeler[f], Neill Barr[f], Mike Harvey[f], Anja Engel[d], Erin Dunne[i], Cliff S. Law[f,g], and Karine Sellegri[a,1]

Edited by Mark Thiemens, University of California, San Diego, CA; received May 25, 2023; accepted October 4, 2023

Our understanding of ocean–cloud interactions and their effect on climate lacks insight into a key pathway: do biogenic marine emissions form new particles in the open ocean atmosphere? Using measurements collected in ship-borne air–sea interface tanks deployed in the Southwestern Pacific Ocean, we identified new particle formation (NPF) during nighttime that was related to plankton community composition. We show that nitrate ions are the only species for which abundance could support NPF rates in our semicontrolled experiments. Nitrate ions also prevailed in the natural pristine marine atmosphere and were elevated under higher sub-10 nm particle concentrations. We hypothesize that these nucleation events were fueled by complex, short-term biogeochemical cycling involving the microbial loop. These findings suggest a new perspective with a previously unidentified role of nitrate of marine biogeochemical origin in aerosol nucleation.

nucleation | marine atmosphere | marine aerosols | nitrate

Significance

Oceans represent 70% of our planet's surface, housing a large spectrum of microorganisms that interact with the above atmosphere. Ocean microorganisms were proposed in the late 80's to be at the center of a climate feedback loop involving dimethyl sulfide (DMS) that would form aerosols and modify cloud properties (CLAW hypothesis). In the present paper, we report observational evidence from semicontrolled experiments in the South Pacific that nitrate ions, yet hitherto not considered, is a key species involved in aerosol nucleation in the pristine marine atmosphere and which precursors are coemitted with DMS. Our results further indicate that nitrate ion formation would be related to short-term microbial processes, sensitive to environmental stressors, therefore potentially "closing the loop".

Interactions between the ocean and the atmosphere are key components of our climate system, not only because of the heat and water vapor fluxes that take place at the interface but also because the oceans are an important natural source of aerosols and trace gases. One pathway by which ocean emissions may influence climate is via the nucleation of trace gases into new nanoparticles and, provided they grow to relevant sizes, the activation of these newly formed aerosols into cloud droplets that subsequently influence cloud properties and lifetime (1, 2). The climate feedback loop described by the CLAW hypothesis (3) suggests that trace-gas emissions from surface ocean microorganisms are modulated by climate change. In response to this hypothesis, studies of the role of ocean biology in the emission of nucleating species have largely focused on dimethylsulfide (DMS), a precursor of methane sulfonic acid (MSA) and SO_2, with the latter being further oxidized to sulfuric acid (SA). In coastal areas, these sulfur compounds have been shown to contribute to marine new particle formation (NPF) (4–7), together with amines (7), ammonia (4, 5), and other organic molecules (5), and iodine products are also considered to play a role (5, 8–10), as well as the presence of charges (4, 5). However, all of these observations were obtained in air masses that had traveled over coastal or ice-bound regions and so are not fully representative of open ocean conditions.

The technical challenges of characterizing NPF in the remote marine atmosphere have hindered the identification of relationships with surface ocean biogeochemistry. Open ocean nucleation and growth as observed in continental environments have rarely been identified in the marine boundary layer (MBL), and so the link to DMS or another precursor of biological origin has been difficult to confirm. However, a recent step forward indicates that nucleation may occur frequently in the MBL with sub-10 nm particle concentrations contributing significantly to total aerosol concentrations [~30% in Southern Ocean air masses (11)]. Furthermore, these new results indicate that the reported rarity of MBL particle production over the open ocean (6, 12) may in fact be due to NPF being systematically overlooked due to the weak intensity and nonconventional nanoparticle growth profile of these events. Here, we report observations from an original experimental setup combined with an unprecedented suite of analytical instruments deployed in the Southwest Pacific Ocean (SWPO) east of New-Zealand during the Sea2Cloud voyage in March 2020 (*SI Appendix*, Fig. S1) to identify the precursors driving open ocean nucleation and their link to marine microorganisms (13).

Results

Particle Formation in Ship-Borne Air–Sea Interfacial Enclosures. Three back-to-back experiments were performed in two shipborne 1.8-m^3 air–sea interface tanks (ASIT) that were half-filled in situ with surface seawater of differing water mass origin, representative

Author contributions: C.S.L. and K. Sellegri designed research; M. Rissanen, T.B., S.I., A.S.-M., M. Rocco, K. Safi, S.D., N.B., M.H., C.S.L., and K. Sellegri performed research; G.C., M. Rissanen, T.B., C.R., S.I., A.S.-M., M. Rocco, and E.D. analyzed data; and G.C., M. Rissanen, T.B., A.S.-L., C.R., S.I., A.S.-M., A.E., E.D., C.S.L., and K. Sellegri wrote the paper.

The authors declare no competing interest.

This article is a PNAS Direct Submission.

Copyright © 2023 the Author(s). Published by PNAS. This open access article is distributed under Creative Commons Attribution-NonCommercial-NoDerivatives License 4.0 (CC BY-NC-ND).

Although PNAS asks authors to adhere to United Nations naming conventions for maps (https://www.un.org/geospatial/mapsgeo), our policy is to publish maps as provided by the authors.

[1]To whom correspondence may be addressed. Email: karine.sellegri@uca.fr.

This article contains supporting information online at https://www.pnas.org/lookup/suppl/doi:10.1073/pnas.2308696120/-/DCSupplemental.

Published November 22, 2023.

Downloaded from https://www.pnas.org by CSIC UNIDAD DE RECURSOS DE INFORMAC on January 26, 2024 from IP address 161.111.20.207.

of subtropical, subantarctic, and frontal regions of the SWPO (*SI Appendix*, Fig. S1). The subantarctic seawater sample was representative of latitudes 45-60S being rich in macronutrients (inorganic N and P) but low in phytoplankton biomass (Chl-a). The subtropical seawater sample was representative of the latitudes 30-45S, being low in dissolved inorganic N and P, which was reflected in lower phytoplankton biomass. Mixing between these two contrasted water types in frontal waters supports blooms of elevated biomass of different phytoplankton groups. Therefore frontal waters in this region are biologically productive. More details on seawater mass biogeochemical properties are given in Sellegri et al. (13).

The ASIT headspaces were flushed continuously with particle-free marine air for the measurement of emission fluxes and subsequent nucleation (*Materials and Methods*). Furthermore, the impact of ozone, a natural oxidant present at low concentrations in the Southern Ocean atmosphere but projected to increase in the future (14), was tested by using one ASIT as a control (ASIT-control) and the other ASIT (termed ASIT-ozone) continuously enriched with ozone, resulting in an additional ~10 parts per billion volume (ppbv) ozone headspace concentration (as compared to the ~6 ppbv ozone concentration measured in the ASIT-Control, *SI Appendix*, Fig. S2).

Increases in the concentrations of particles >1 nm (N1) relative to those in the incoming sheath air provide evidence for the occurrence of NPF in the headspace of the frontal water sample in Experiment A (Fig. 1*B*). Calculated N1 formation rates (Eq. **S1**) are consistent (within 50%) with that of sub-10-nm nanoparticle concentrations reported for the open Southern Ocean (11) and in pristine Antarctic air (15). Nucleation was also observed in Experiment B with sub-Antarctic water, at rates 6 times lower than with frontal water, whereas there was no nucleation during the subtropical water incubation (Experiment C). Growth of the newly formed particles was observed within the 40-min residence time in the ASIT headspace as N3 and N10 concentration time series resembled those of N1, albeit at lower concentrations (correlations shown in *SI Appendix*, Fig. S3). Unexpectedly, nucleation was observed primarily during nighttime and continued to decrease for a few hours after sunrise, whereas the vast majority of NPF events reported in terrestrial environments are initiated after sunrise (15). In addition, the nighttime formation of particles was systematically lower in the ASIT-ozone relative to the ASIT-control in both experiments in which nucleation occurred. This apparent inhibitory effect of ozone was also unexpected, particularly at nighttime when its role as an oxidant leading to aerosol formation is typically strongest (16, 17).

VOC and Molecular Cluster Composition. Most of the measured VOCs (DMS, monoterpenes, isoprene, and iodomethane) showed positive fluxes to the atmosphere, and higher concentrations in the frontal water experiment (*SI Appendix*, Fig. S2). Of these, DMS closely followed the concentration profile of nanoparticles in both ASITs. However, the major oxidation products of DMS, namely SA and MSA, were not enhanced above background (sheath air) in the ASITs headspace. The absence of strong MSA and SA signals may be due to a number of factors including the relatively low reactivity of DMS (18) combined to the short residence time (<40 min) of air in the ASITs which prevented significant populations of nucleating clusters from accumulating. Recent studies have identified hydroperoxymethyl thioformate (HPMTF; $HOOCH_2SCHO$) as another abundant DMS oxidation product (18, 19), although this was not detected in the headspace, either due to HPMTF solubility in water or due to low detection sensitivity of nitrate chemical ionisation mass spectrometer (CIMS) (20).

Analysis of the chemical composition of neutral molecular clusters using a nitrate chemical ionisation atmospheric pressure ionisation time-of-flight mass spectrometer (CI-API-ToF-MS, hereafter abbreviated to CIMS) and precursor gases by proton transfer reaction mass spectrometry (PTR-MS) (see *Materials and Methods* and *SI Appendix*, section S1) provides information on the chemical processes occurring in the initial 40 min following precursor emissions. We show the time evolution of molecular clusters grouped in families (*Materials and Methods* and *SI Appendix*, Table S1) based on cross-correlations of each mass peak identified as enriched or lost in the headspace (*SI Appendix*, Fig. S4). Iodomethane was elevated during nanoparticle formation with the frontal water experiment although we did not detect iodine in the form of iodic acid, as previously identified using the nitrate-CIMS technique during daytime particle formation events in coastal areas (5, 9). Maleate, malonate, and highly oxygenated organic molecules (HOM), which are compounds that participate in nighttime nucleation in other environments (21), were observed at low concentrations with a slight increase coincident with nanoparticle formation with the frontal water sample; however, these species showed similar concentrations in the two ASITs, inconsistent with the higher nucleation rates in the ASIT-control. C_2–C_6 amines were detected in the headspaces at higher concentrations than in flushing air, indicating emission from the seawater, where they are produced by marine biota; however, headspace concentrations were similar in all three experiments, suggesting that amine availability was not a limiting factor for nucleation. Carbamide/urea [$CO(NH_2)_2$] was also enriched in the headspace, with a temporal evolution similar to that of amines indicating similar production and emission processes.

Water clustering with the reactant ion [$(H_2O)_nNO_3$] was stronger in the headspaces compared to flushing air, probably due to higher humidity, and showed a significant correlation with nanoparticle concentrations ($r = 0.57$ for Control and $r = 0.33$ for Ozone, both with P value $\ll 0.01$). Although some of the identified neutral molecular clusters cited above may contribute to particle formation, none reflected the large increase in 1 to 3 nm particle concentration observed in the ASIT-control during the frontal waters incubation (Fig. 1). We cannot exclude significant losses of more condensable species in the sampling lines (*Materials and Methods*), as the observed concentrations of chemicals and nanoparticles were typically low. Note that although not enriched, SA was detected in the ASIT's headspace and so any other species of similar mass range, very low vapor pressure, and high surface activity should have been detected at equivalent concentrations to SA, provided the species has proton affinity larger than HNO3 or bonds strongly with the nitrate ion.

An explanation for the absence of neutral clusters in the range <200 amu correlating with 1 to 3 nm particle formation is that the chemical ionization of neutral molecular clusters was determined analytically using nitrate as an ionizing agent in the negative ion mode. In order to overcome the bias in cluster detection due to chemical ionization, we investigated the composition of the naturally charged molecular clusters in the Api-ToF. The only species detected in high abundance was the nitrate ion (NO_3^-) and the nitrate dimer ($HNO_3NO_3^-$) (*SI Appendix*, Fig. S5). The concentrations of the nitrate ion and its dimer were highly correlated with the 1 to 3 nm particle concentration (*SI Appendix*, Fig. S6), particularly in the ASIT-control, in all three experiments ($r = 0.94$ for Control and $r = 0.33$ for Ozone, both with P value < 0.01), strongly implicating their involvement in the nucleation process.

Potential Nucleating Mechanisms Involving Nitrate Ion. Observations suggest that organo-nitrates ($RONO_2$) may be the dominant form of reactive nitrogen in remote marine environments

Downloaded from https://www.pnas.org by CSIC UNIDAD DE RECURSOS DE INFORMAC on January 26, 2024 from IP address 161.111.20.207.

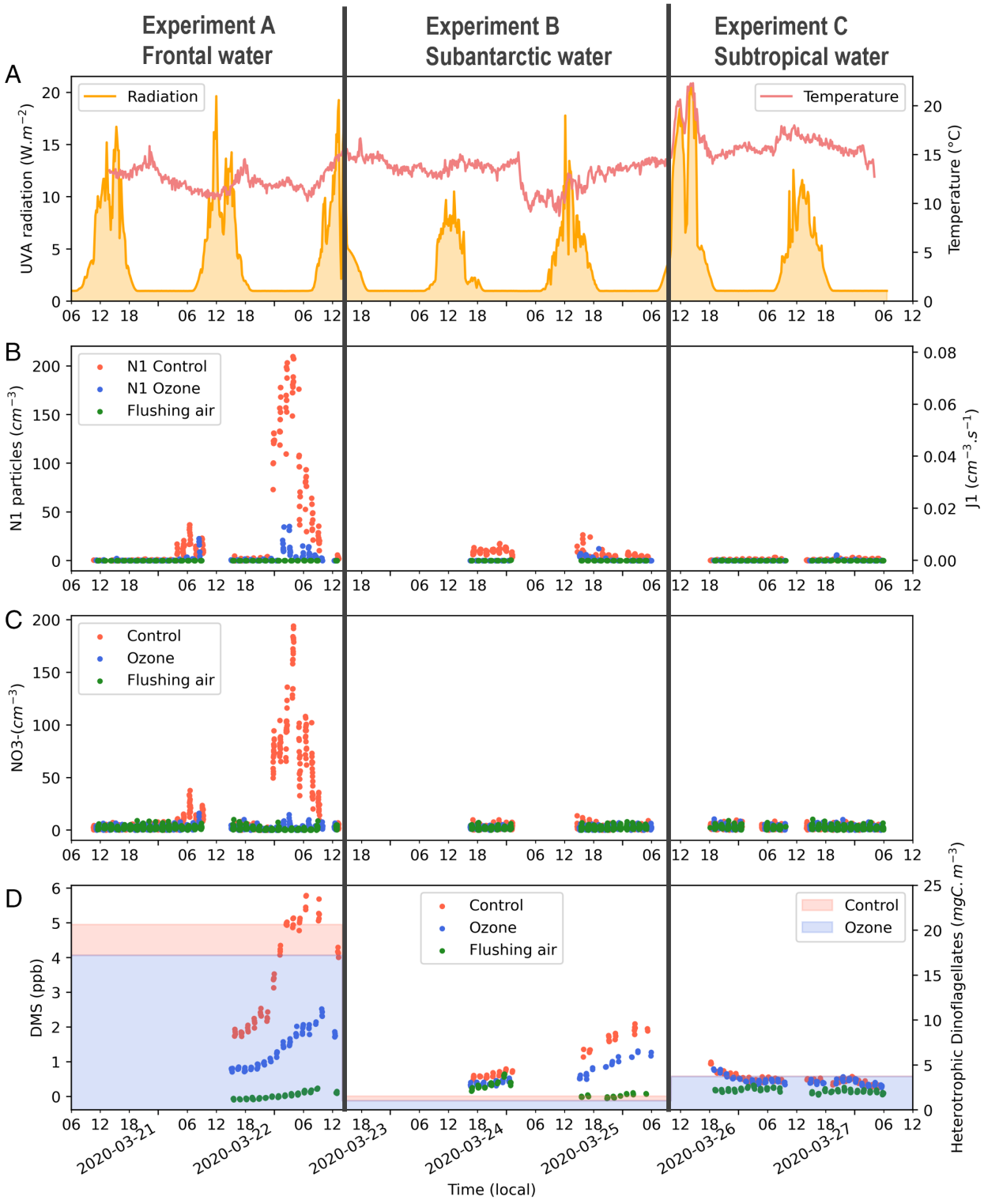

Fig. 1. Variables measured in the ASITs headspace: (*A*) incoming UVA radiation (W,m^{-2}) and air temperature (°C) (*B*) concentration of particles with diameters larger than 1 nm (N1) corrected for estimated losses and corresponding formation rates (J1) calculated following Eq. **S1**. (*C*) Nitrate-ion concentrations (NO_3^-) (cm^{-3}) corrected for estimated losses (*Materials and Methods*), (*D*) DMS concentration (ppb, filled circles) and seawater heterotrophic dinoflagellates biomass averaged over each experiment (mgC m$^{-3,}$ shaded horizontal bars).

(22). Organo-nitrate may be formed from the reaction of the nitrate radical with VOCs. Nitrate radicals show a high reactivity with unsaturated hydrocarbons such as monoterpenes, which were detected at higher concentrations (~2 ppb) in the ASIT-control and EXP A. However, the potential ability of organo-nitrates to nucleate at night was shown less likely than the nucleation from nonnitrogenous oxidation products (21, 23). Moreover, the presence of organo-nitrates is not expected to give a high NO_3^- signal in the Api-ToF-MS (*SI Appendix*, section S3).

Nitrate ions may indicate the presence of nitric acid. Nitric acid has not generally been considered as playing a role in NPF events due to its relatively high vapor pressure. However, nitric acid has the ability to form strong primary acid-base clusters, hydrogen-bonded networks, and ultimately salts (24–26). Recently, nitric acid has been

Downloaded from https://www.pnas.org by CSIC UNIDAD DE RECURSOS DE INFORMAC on January 26, 2024 from IP address 161.111.20.207.

observed to nucleate with ammonia in simulated urban cold updraft conditions (27). It also has potential involvement in stabilizing atmospheric clusters initiating NPF in other systems, as it is highly acidic and contains both hydrogen bond donor and acceptor sites, making it a good building block for ambient multicomponent clustering. Ammonia (NH_3) was not detected, yet fingerprints of several amines were present in the neutral clusters measured with the CIMS (e.g., urea [$(O)C(NH_2)_2$] and dimethylamine [$(CH_3)_2NH$] *SI Appendix*, Fig. S4). Considering the HNO_3 molecular structure, amines could produce more stable and so more favorable clusters with HNO_3 than NH_3, and indeed, amine detection by nitrate CIMS has been reported previously (7) and in the present experiments. Additionally, aliphatic amines form salts with nitric acid (24):

$$NR_{3(g)} + HNO_{3(g)} \leftrightarrow HNR_3NO_{3(s)} \rightarrow HNR^+_{3(aq)} + NO^-_{3(aq)}. \quad [\mathbf{R1}]$$

A previous theoretical study (26) has shown that the nitric acid-dimethylamine heterodimer cluster is weakly bound, with a Gibbs free formation energy of −5.7 kcal/mol at 298.15 K and a corresponding evaporation rate of 7×10^5 s^{-1}. Once formed, the cluster containing two nitric acid and two dimethylamine molecules has an evaporation rate that is ~7 orders of magnitude lower than the heterodimer. Gas-phase urea [$(O)C(NH_2)_2$] was also detected by the nitrate-CIMS instrument during the experiments indicating a potential role in particle production; we therefore investigated the stabilities of nitric acid–urea clusters using quantum chemical methods (*SI Appendix*, Fig. S7 and *Material and Methods*) but found the potential clusters unlikely to contribute to nanoparticle formation on their own (*SI Appendix*, section S2).

Stability of newly formed clusters can be enhanced by the presence of natural charges (28), with ion-induced nucleation reportedly representing almost 100% of NPF in the Arctic (5). In the present experiment, calculated nitrate ion concentrations were of the same order of magnitude (50 to 200 cm^{-3}) as the N1-3 concentrations during the peak of the particle production with frontal waters, further suggesting that nitrate ion-induced nucleation may be a prevalent nucleation path in the remote open ocean atmosphere at nighttime. The absence of further neutral clusters in the CIMS spectra likely results from their steady-state concentrations being too low in the high condensational sink (CS) environment of the ASIT, or potentially, the NO_3^- ionization scheme employed in the CIMS is not ideal for detecting them. Note that the ions postulated to have importance for the observed events (i.e., NO_3^- and $HNO_3NO_3^-$) are naturally masked in the nitrate CIMS by the reagent ion peaks.The vast majority of (if not all) CIMS measurements to characterize NPF in chamber experiments (29–32) and natural environments influenced by marine air masses (5–7, 9) were performed using nitrate as an ionizing agent. In fact, we did not find any CIMS measurements in the pristine marine atmosphere that did not use nitrate as an ionizing agent, which may explain why it has been previously overlooked.

It is instructive to note that nitrate ion–based chemical ionization was practically invented due to its prevalence as a natural atmospheric ion (33). Subsequently, nitrate was observed to be the prevalent ion attached to HOMs [the fuel for growing ambient nanoparticles (34)] and also attached to carboxylic acid, iodic acid, and MSA in the early morning stable boundary layer of the boreal forest (35). Thus, the involvement of nitrate ions in NPF could be more common than generally assumed. It should also be noted that the concentration of common sulfur-containing clusters that are often related to NPF events was almost absent in the ASIT experiments, which could be part of the reason why the nitrate ions were so pronounced, as sulfur compounds are known to "steal the charge" due to their high electron affinities (33, 36).

The nitrate radical is the key species oxidizing DMS or other VOCs to form HNO_3 [following R2; (37)]:

$$NO_3 + DMS/VOC \rightarrow HNO_3 + products(RO_2). \quad [\mathbf{R2}]$$

This may explain why DMS was correlated with cluster formation (r = 0.72) without any DMS oxidation products being detected.

Relevance for Ambient Air Nucleation Over Open Oceans of the Southern Hemisphere. While the ASITs experiments were useful for directly observing linkages between biogeochemical conditions and air–sea interactions, they are not fully representative of open ocean conditions. The ASIT's headspaces were more concentrated with respect to condensable gaseous precursors than the surrounding ambient atmosphere. DMS concentrations reached 6 ppbv in the ASIT-control headspace, whereas it was always lower than 1 ppbv in the ambient air (38). This is due to lower ventilation in the ASIT, which was estimated to be equivalent to very low wind speeds of ~0.6 m s^{-1} (38). The enhanced headspace concentrations would then favor nucleation relative to the concentrations in natural ambient air; however, this would have been counteracted by the short residence time in the ASIT headspace (~40 min) for primary emissions to be oxidized to lower volatility compounds and also by the higher CS related to the ASITs walls (see CS calculation *SI Appendix*, section S3).

To explore whether these nitrate ion–based nucleation processes may be occurring over the open ocean, ambient aerosol data from the voyage, and also 2 coastal sites (Baring Head and Maïdo) during periods when unperturbed marine air masses (free from ship exhaust and land influences), were examined for evidence of nucleation events. During the 10-d voyage, several periods of remote marine air masses were observed, including one full day without ship contamination during which night-time NPF was observed; *SI Appendix*, Fig. S8 shows a time series of the particle number size distribution and $N_{3\text{-}10}$ measured by the particle size magnifier (PSM) and scanning mobility particle sizer (SMPS) (*Material and Methods*) with pure marine air masses. The $N_{3\text{-}10}$ concentration reached a maximum of 300 cm^{-3} at 06:00 and a slow growth of the newly formed ultrafine particles was observed later during the day, from 10 nm to 25 nm, indicating survival up to climate-relevant sizes. Unfortunately, the ambient air sampling lines prevented detection of ions by the API-ToF during the voyage.

Statistical analysis of a 10-mo dataset collected at Baring Head, New-Zealand (−41.40°, 174.87°), showed that sub-10 nm particle concentrations increased in the hours prior to sunrise in southerly air masses from the remote Southern Ocean (11), together with a peak in nitrate ions (39), consistent with the observations in the ASIT experiments. We calculated that nighttime (00:00 to 05:00 LT) nitrate ions represented about half of the identified ions when sub-10 nm particle concentrations were <500 cm^{-3}, increasing to around 70% when sub-10 nm particle concentrations were >500 cm^{-3} (Fig. 2). The nighttime nucleated clusters are likely to grow and survive as sub-10 nm particles and represented 30% of the total aerosol (including sea spray) concentrations during daytime (11). Previous studies in the North Atlantic have shown that these types of clusters may experience further growth over several days to climate-relevant sizes of a few tens of nanometers (12).

The same prevalence of nitrate ions was observed in ion composition (*Materials and Methods*) in the free troposphere at night at the Maido observatory (−21.08°, 55.38°) on Reunion Island in the Indian tropical ocean at 2,150 m a.s.l., although the restricted measurement period (6 d) did not allow for the observation of a NPF event to confirm it was accompanied by an increase of nitrate ion clusters.

Downloaded from https://www.pnas.org by CSIC UNIDAD DE RECURSOS DE INFORMAC on January 26, 2024 from IP address 161.111.20.207.

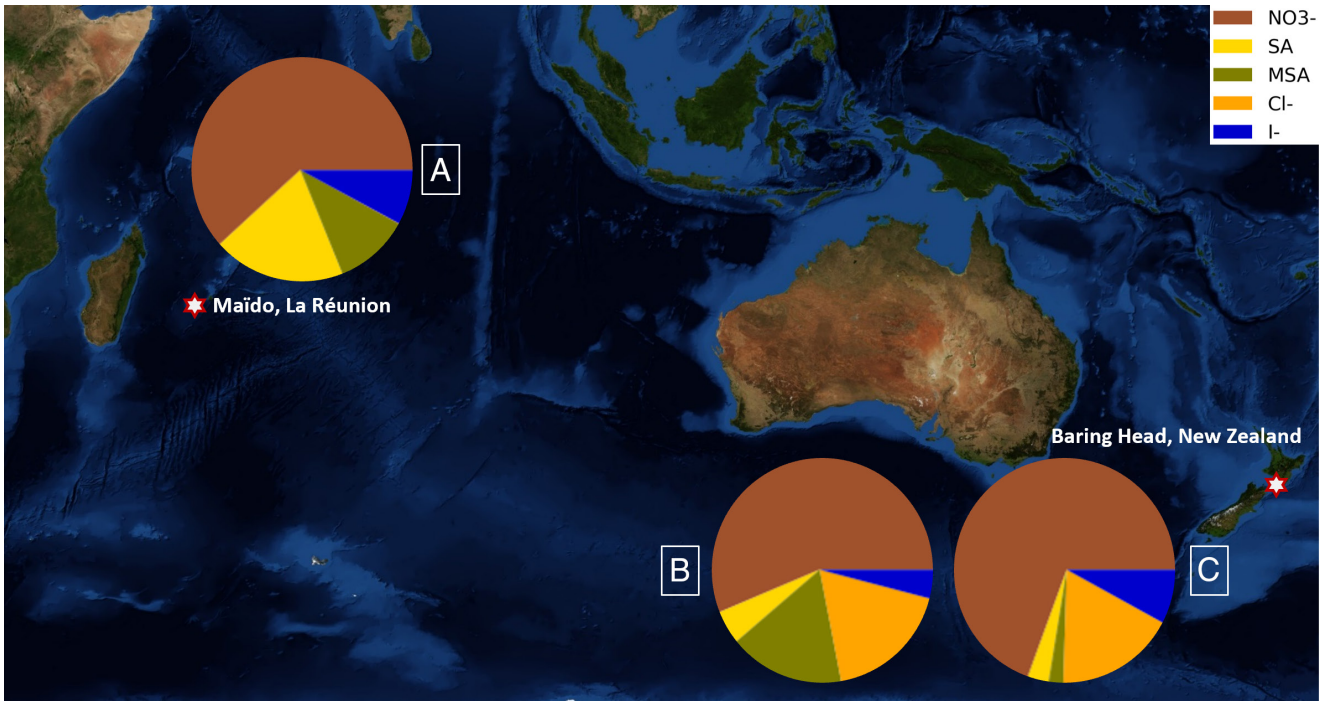

Fig. 2. Nighttime ion cluster composition measured by API-ToF-MS in pristine marine air masses at Maïdo, La Réunion (*A*) and Baring Head, New Zealand, for low sub-10 nm particle concentration ($N_{1\text{-}10} < 500\ cm^{-3}$) (*B*) and high sub-10 nm particle concentration ($N_{1\text{-}10} > 500\ cm^{-3}$) (*C*). SA: bisulphate, MSA: Methanesulfonate, Cl:Chloride, I: Iodide. Ion groupings are explained in (*SI Appendix*). The total of peaks presented accounted for 15 to 20% of the TIC (total ion current) from Maïdo and ~15% from BH and included the most abundant compounds for m/z <200 amu. Details of peaks accounting for SA and MSA are shown in *SI Appendix*, Table S1.

On the Origin of Nitrate Precursors. A key step in understanding the potential of this NPF process is to track the availability of the initiating nitrate radical. Gas–liquid phase equilibrium of HNO_3 dictates that almost all of the nitric acid will be in the aqueous phase under conditions of the ASIT (40). Therefore, nitrate radicals are the most plausible source of the gas-phase nitric acid and were most likely formed within ASIT's headspace from other nitrogen compounds degassing from the seawater. Candidates for degassing nitrate radical precursors from the seawater include NO (potential degassing short-chain alkyl nitrates are discussed in *SI Appendix*, section S5).

NO is a sparingly soluble gas that can be degassed to the atmosphere when supersaturated in seawater (40). The chemical reactions leading to the formation of NO_3 radical from NO in the gas phase would first require oxidation to NO_2 and then to the nitrate radical via

$$NO + O_3 \rightarrow NO_2 + O_2, \qquad [\mathbf{R3}]$$

$$NO_2 + O_3 \rightarrow NO_3 + O_2. \qquad [\mathbf{R3'}]$$

Since NO_3^- is detected with higher concentrations in the ASIT-control headspace compared to the ASIT-O_3, we hypothesize that NO emissions are stronger in the ASIT-control and compensate for lower ozone concentrations.

Tian et al. (41) have reported an unidentified nighttime source of NO from the Bohai and Yellow Seas east of the Chinese coast, unrelated to abiotic photoproduction, and supersaturated in the surface seawater. Phytoplankton produce antioxidants, including NO, to combat stress-induced reactive oxygen species (ROS) (42, 43). The release of ROS is induced by environmental stressors such as grazing, viral infection (42), or in response to signaling molecules (44, 45). Elevated intracellular levels of NO and ROS favor the production of peroxynitrite ($ONOO^-$), which ultimately initiates programmed cell death in phytoplankton cells (46). Additionally, heterotrophic bacteria can rapidly consume labile dissolved organic matter (DOM) released by phytoplankton within minutes to hours (47, 48) and utilize NO synthases which catalyze NO from amino acids present in labile DOM (49, 50). Various microbial pathways have been identified that produce NO, including nitrification and denitrification (51–54), representing alternative microbial sources of NO. Although denitrification is not expected in surface waters, it was recently shown as a potential route for the bacterial reduction of NO_2 to NO under oxygen-rich conditions (51). Indeed, dissolved nitrite (NO_2^-), an intermediate in some of these pathways and a source of NO, is present in elevated concentrations in surface frontal waters east of New Zealand (55). Analogous to marine biogenic production of NO, phytoplankton also produce dimethylsulfoniopropionate (DMSP) which is released into seawater as a result of exudation, senescence, grazing, or viral lysis and is converted to DMS via bacterial catabolism. Overall, the biologically mediated processes involved in the production and release of intracellular NO, DMSP, and other DOM into the surrounding seawater are likely to be key to the availability of the nucleation precursors identified in this study. Indeed, changes in DMS headspace concentrations reasonably followed nighttime nucleation events in both ASITs (Fig. 1), indicative of the common waterside production pathways of cluster precursors as well as their proposed respective roles in the atmospheric nucleation pathways.

Elevated dissolved DMSP concentrations and heterotrophic dinoflagellate biomass were present in the frontal water in Exp A, reflecting the capacity of this phytoplankton group to synthesize DMSP (56). This elevated heterotrophic dinoflagellate biomass in frontal waters in Exp A was also associated with higher dissolved DMS concentrations, potentially reflecting the capacity of this phytoplankton group to directly cleave DMSP into DMS (*SI Appendix*, section S6). Headspace NO_3^- concentration also

Downloaded from https://www.pnas.org by CSIC UNIDAD DE RECURSOS DE INFORMAC on January 26, 2024 from IP address 161.111.20.207.

showed a significant correlation with heterotrophic dinoflagellate biomass (r = 0.61; $P < 0.05$, *SI Appendix*, Fig. S9), which may indicate that the release of DMSP, DMS, NO, and also DOM results from heterotrophic dinoflagellate grazing on other phytoplankton (57) (*SI Appendix*, section S4).

In Exp A, DMS emissions and NO_3^- production in the Control were greater on the second night (22nd of March) than on the first night (21st of March) of the incubation. As the composition of the flushing air was not altered (Fig. 1 *C* and *D*) and thermodynamical equilibrium was reached within the average residence time (~40 min), this indicates a change in precursor production in the water that may reflect increased stress over the course of the experiment, as corroborated by elevated dissolved DMS in the seawater on the 2nd day (*SI Appendix*, Fig. S10) [see *SI Appendix*, section S6 and Rocco et al. (38)].

We also observe that although heterotrophic dinoflagellate biomass in the frontal water greatly exceeded that of the sub-Antarctic and subtropical waters, the difference in heterotrophic dinoflagellate biomass between the ASIT-control and ASIT-ozone was lower. Therefore, differences in the headspace NO_3^- and DMS concentrations between the two ASITs may be attributed to differences in the production of DMS and coemission of NO in the ASIT-control headspace under increased stress. Measurements of DMS and DMSP in the seawater show a difference in these concentrations between the ASIT-control and ASIT-ozone (*SI Appendix*, Figs. S10 and S11). Also, we did not find any significant differences in the ratio of DMS concentrations in the ASIT's headspace to DMS in the seawater between the ASIT-control and the ASIT-ozone, indicating that ozone chemistry had little impact on the DMS and likely NO_3^- headspace concentration. Therefore, there are strong indications that ozone is actually acting on the biological processes in the seawater. Stress could potentially be due to dinoflagellates receiving more UV in the ASIT-control than in the ASIT-ozone or due to ozone limitation of biologically mediated processes controlling the release of intracellular NO, DOM, and DMSP (viruses or grazing) and/or of the conversion of DOM to NO and DMSP to DMS in seawater (bacterial).

Discussion

The potential role of nitric acid and nitrate ion in the formation of new marine aerosol particles has been largely neglected to date. We suggest that because the vast majority of chemical ionization mass spectrometry (CIMS) studies of NPF have used nitrate-based chemical ionization (5–7, 9), the role of nitrate ions in nucleation in the marine atmosphere has so far been overlooked. While the ocean is recognized as a source of atmospheric organic nitrogen compounds (e.g., alkyl nitrates, aliphatic amines, and urea) and ammonia (NH_3) (58), and nitrogen-containing aerosols are preferentially produced relative to organic carbon in the marine atmosphere, the origin and formation processes of marine nitrate aerosols remain unresolved (59). With the present paper, we suggest that a potentially important, hitherto unrecognized pathway for nucleation to occur in the open ocean boundary layer, is induced or mediated by nitrates of biogenic origin (Fig. 3). Our observations suggest that the nitrate ion's abundance is not elevated during the day but preferentially in the hours preceding dawn. Our observationally based hypothesis, which calls for further investigation, is that the stress-related biological processes leading to the formation of NO_3^- involve NO, another generally overlooked species in the ocean nitrogen cycling. The lack of nitrogen-based nucleation during daytime is due to the NO_3 radical being readily photolyzed and also due to NO emissions being dominant during nighttime. This is supported by the observations of Tian et al. (41) and also other process-based studies that report viral lysis as a significant environmental stressor (60) that predominantly occurs at night (61) and favors the production and release of NO (42), DMSP, and DOM.

As it is not known how future changes in ocean temperature, ozone concentration, and light availability will impact surface ocean microbial processes and community composition and subsequently influence the emission of nitrogen compounds, further research is required to quantify the magnitude of this potential NPF source and to assess its potential importance in a changing climate. Field studies are needed to evaluate in which form reactive nitrogen is produced in the seawater and emitted to the atmosphere, with laboratory studies required to evaluate the factors controlling the atmospheric emissions of reactive nitrogen.

The high correlation between DMS, NO_3^-, and N1 particles provides an interesting new perspective on the CLAW hypothesis, in which DMS may only be indirectly involved in marine aerosol nucleation. However, the exact role of DMS and other marine VOCs, either coemitted with NO, and/or playing a dominant role in the gas-phase oxidation of NO to HNO_3, also needs to be further investigated. Our system allowed us to study the very first steps of nucleation, but it is possible that the detected amines emitted from seawater could contribute to further cluster growth, due to their well-known tendency to cluster with strong acids, including HNO_3. Also, the fast oxidation of amines during daytime (i.e., mainly OH oxidation, but also slow O_3 reactions) forms basic compounds that may participate in ambient particle formation [e.g., double-bonded imines (24, 62)] potentially up to cloud condensation nuclei (CCN) sizes.

According to model estimates, nucleation followed by growth contributes to more than half of the total aerosol particle number and therefore CCN in the atmosphere, with only DMS oxidation included as a marine new particle source (63). Nitric acid and nitrate ion–based nighttime nucleation is currently omitted in chemistry-climate models and consequently requires further evaluation to determine its significance and implications for climate.

Materials and Methods

Ship-Borne ASIT Experiments. The ASITs experiments were performed in March 2020 as part of the Sea2Cloud campaign in the SWPO onboard the RV *Tangaroa*. All experimental and analytical procedures are detailed in Sellegri et al. (14). Briefly, the ASIT was designed for observing air–sea interactions and NPF from marine emissions. These 1,820 L tanks were half-filled with open ocean waters from the Chatham Rise area, East of New-Zealand (*SI Appendix*, Fig. S1), and their headspace continuously flushed with clean ambient filtered air. The flushing flow rate was 26 LPM, resulting in a residence time of around 40 min. Tanks were air-tight with a pressure valve, and a slight overpressure was imposed to further prevent potential external contaminations.

A four-port entrance electrovalve switched every 20 min between the two ASITs, ambient air and flushing air, allowing stepwise analysis of their composition using a single analytical instrumental setup (*SI Appendix*, Fig. S12). The online analytical instrumental setup comprised gas-phase, aerosol-phase, and cluster instrumentation. Newly formed aerosol concentrations were measured using a PSM [Airmodus A10 (52)] operated in a stepping mode (with respectively, 1 nm and 2.5 nm size cuts) (64) and a Condensation Particle Counter (CPC, TSI 3010) with a size cut of 10 nm (65). The ozone concentration (66) was measured with a Thermo Scientific Model 49i Ozone Analyzer, SO_2 (67) with a Thermo Scientific Model 43i SO_2 Analyzer, and VOC composition (68) with a proton-transfer reaction-mass spectrometer (PTR-MS, Ionicon Analytik, Innsbruck, Austria). Further details on the PTR-MS measurements can be found in Rocco et al. (69). In the ASIT-ozone, ozone was added with a 1 LPM flow at 100 ppb generated using a Teledyne Instruments Model 700E Dynamic Dilution Calibrator.

Downloaded from https://www.pnas.org by CSIC UNIDAD DE RECURSOS DE INFORMAC on January 26, 2024 from IP address 161.111.20.207.

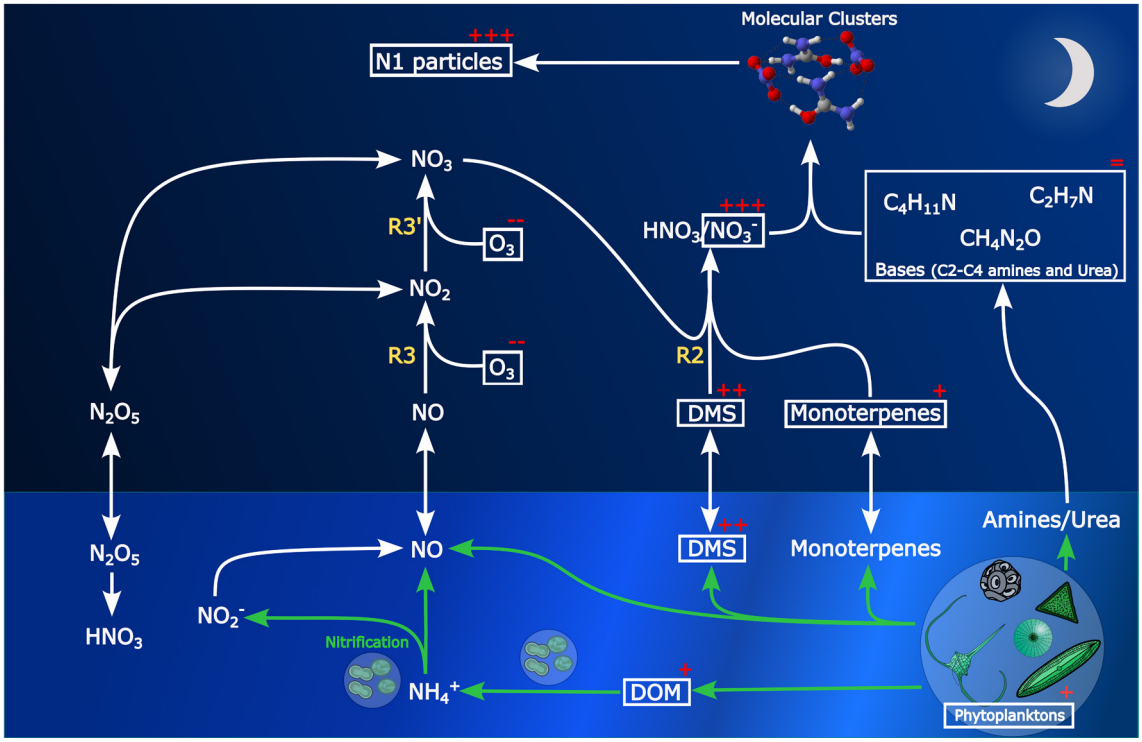

Fig. 3. Schematic of the potential pathways for the formation of nitrate-induced clusters leading to particle formation. Reactions referring to text are written in yellow, and emission and reaction associated with biological processes appear in green. Species measured are indicated with a white frame. Species enriched in the ASIT-control compared to ASIT-ozone are denoted with the symbol + and those depleted with a symbol −, the values are shown in *SI Appendix*, Figs. S2 and S11.

Two mass spectrometers were used to measure the composition of newly formed clusters. The chemical composition of neutral molecular clusters (70) was measured with a nitrate chemical ionization atmospheric pressure interface time-of-flight mass spectrometers [CI-API-ToF-MS, abbreviated as CIMS, TofWerk AG, (71)], while the natural ion chemical composition (72) was measured with an API-Tof-MS [Aerodyne, (73)] operated in the negative ion mode.

Estimates of particle losses in the sampling lines by diffusion were calculated using the formula from Willeke and Baron (74), giving a transmission efficiency of 15% for N1–3 concentrations. As we do not know the aerosol size distribution above 3 nm, N1 concentrations were calculated by adding uncorrected N3 to the N1–3 concentrations corrected for losses. Hence N1 are underestimations of the real N1 concentrations. The measured nitrate ion concentrations can be estimated by considering the nitrate ion transmission efficiency in the API-ToF-MS, reported to range between 0.1% and 0.5% for Api-ToF instruments (73). For calculating nitrate ion concentrations, we used a transmission efficiency in the instrument of 0.5%, as a lower limit of the nitrate losses in the instrument. Losses of nitrate ions in sampling lines were approximated to 96% as the 1 nm particles which are giving a 0.02% transmission efficiency through lines and instruments. Hence, estimated nitrate ion concentrations provided after correction are lower limits of the real concentrations and fluxes. The detection limit of neutral clusters is five orders of magnitude lower than that of natural ions, due to the chemical ionization technique (75), and more compounds are detected in the CIMS mode compared to API-ToF-MS mode. Here, we should note that SA signals were not abundant but were above the instrument's detection limit, and given the very low volatility of SA, any compound of similar concentration should be detected. Amines were detected at higher concentrations in the ASIT's headspace than in the flushing air (which can be regarded as a blank or a reference), therefore we exclude they are issued from contaminations from the sampling lines and valves. We should also note that given the residence time of ~40 min in the ASITs headspaces, we cannot observe significant cluster growth that would take a longer time than this residence time. Also, switching the valve every 20 min prevented the extraction of a mass defect plot of cluster growth as usually performed in Api-Tof measurements of ambient air.

Three experiments were performed with contrasted seawaters of differing origins. Experiment A run from 20 March to 22 March 2020 23:00 local time (LT), with seawaters of frontal origin, Experiment B run from 23 March 06:00 LT to 25 March 2020 06:00 LT with seawaters of sub-Antarctic origin, and experiment C run from 25 March 15:00 LT to 27 March 2020 06:00 LT, with seawater of subtropical origin (*SI Appendix*, Fig. S1). Following each 2-d experiment, the ASIT tank was drained and cleaned. Measurements of water composition were carried out in both ASITs at time zero [measurement detailed in Sellegri et al. (13)], 24 h, and 48 h (end of the experiment). We obtained data for water composition including Chlorophyll-a (Chl-a), particulate nitrogen and carbon (PN and PC), pigments, chromophoric DOM, DOM composition including dissolved organic carbon, dissolved amino acids and carbohydrates, and microbial community composition (flow cytometry (76), flowcam (77), and microscopy).

Ground-Based Field Campaign at Maïdo. Measurements were performed at the Maïdo observatory located on Réunion island (21.080°S, 55.383°E; 2,150 m a.s.l.), in the Indian Ocean, during the OCTAVE (oxygenated organic compounds in the tropical atmosphere: variability and atmosphere–biosphere exchanges; http://octave.aeronomie.be) measurement campaign that took place between March and May 2018. In addition to the instrumental setup which is in continuous operation at this GAW (Global Atmospheric Watch) site for monitoring the properties of atmospheric aerosol particles and gases, instruments allowing a detailed physicochemical characterization of cluster particles and their precursors were deployed during this period. In particular, the number size distributions of ions in the electrical mobility range 3.2 to 0.0013 $cm^2\ V^{-1}\ s^{-1}$ and particles in the size range ~2 to 42 nm were measured with a neutral cluster and air ion spectrometer [NAIS (78)]. In addition, the chemical composition of natural ions was measured with an API-ToF-MS (73). The data used in this study are from the period between April 24 and 30 (79).

To avoid the presence of local terrestrial sources (natural or anthropogenic) of precursors interfering with the identification of the compounds of marine origin of interest for this study, the analysis was limited to periods during which the station was in free tropospheric conditions, under the influence of large-scale subtropical subsidence. Based on the study of Rose et al. (80), the SD of the horizontal wind direction was used to detect such conditions; the value of 16° was identified as a reasonable threshold below which conditions are considered representative of the free troposphere at this site. Consistent with previous observations at other mountain sites, these conditions are mainly observed at night (80–82). The data were finally filtered based on the SO_2 mixing ratios measured

Downloaded from https://www.pnas.org by CSIC UNIDAD DE RECURSOS DE INFORMAC on January 26, 2024 from IP address 161.111.20.207.

at the site to exclude periods during which the measurements may have been affected by the eruption of the Piton de la Fournaise which started on April 28. The 2 ppb threshold identified by Foucart et al. (83) and since used by Rose et al. (84) was also applied here; only the measurements corresponding to SO_2 levels below this value were kept in the analysis.

Ground-Based Field Campaign at Baring Head. Experimental and analytical details on measurements performed at Baring Head can be found in Peltola et al. (11) and Peltola et al. (39). Briefly, Baring Head is a coastal measurement station located in New Zealand (41.4083°S, 174.8710°E). This site regularly receives air masses from the Southern Ocean free from land influence in the last days.

The instrumental setup in the Baring Head station included SMPS, NAIS, PSM (85), CPC (86), and an API-ToF-MS (without chemical ionization (87)). PSM, CPC, and API-ToF-MS were the same as those used during the ASITs experiments. Measurements were performed from June 2020 to July 2021.

Baring Head data used in this study are only the data classified as clean marine air based on their back trajectories, radon concentrations, and the wind direction [methodology in Peltola et al. (11)]. The clean marine air masses represent 7.3% of total data (79).

Particle Formation Rate. Particle formation rates were calculated for the Baring Head ambient air dataset and for the ASITs experiments. In order to consider the residence time in the ASITs, we used a balance equation in an unsteady state to determine the production rate of n1 particles (J).

$$V\frac{dc}{dt} = \sum \text{source} - \sum sink, \qquad [\mathbf{S1}]$$

$$\sum \text{source} = C_{inlet}Q + J,$$

$$\sum sink = C_{out}Q + L.$$

Here, C is the concentration of particles measured, V is the volume of the ASITs' headspace, Q is the flushing air flow rate, and L losses. Losses by diffusion inside the ASIT's headspace are not taken into account, which leaves us with, again, a lower limit of the formation rate.

Computational Method. For generating the urea–HNO_3 clusters (*SI Appendix*, Fig. S7), the cluster sampling algorithm ABCluster (88, 89) was applied to generate a series of conformers. The program uses the initial (rigid) geometries of the individual molecules in the cluster, and the partial charges, and the Lennard-Jones potentials of the individual atoms. The partial charges are calculated at the ωB97X-D/aug-cc-pVTZ level of theory by running a single-point calculation with the Pop=MKUFF keyword. The ABCluster procedure uses the force-field method Chemistry of HARvard Macromolecular Mechanics (CHARMM) (90) to generate a list of energetically favorable conformers. These conformers are then optimized using density function theory (DFT) methods at the B3LYP/6-31+G* level. Conformers within 3 kcal mol^{-1} in relative electronic energies are then optimized using a higher DFT ωB97X-D//aug-cc-pVTZ method. A final coupled-cluster single-point energy calculation on the lowest energy geometries is carried out with the domain-based local pair natural orbital coupled-cluster singles, doubles, and perturbative triples [DLPNO-CCSD(T)] method and the aug-cc-pVTZ basis set using the ORCA program (91).

Data, Materials, and Software Availability. ERC Sea2Cloud data have been deposited in Data-Terra (https://sea2cloud.data-terra.org), ASITs API-ToF data ara available at https://doi.org/10.6096/4015 (72) and CIMS data at https://doi.org/10.6096/4014 (70). ASIT PSM data can be accessed at https://doi.org/10.6096/4009 (64), CPC data at https://doi.org/10.6096/4011 (65), PTR-MS data can be downloaded at https://doi.org/10.6096/4010 (68), O3 analyzer at https://doi.org/10.6096/4013 (66) and SO2 analyzer at https://doi.org/10.6096/4012 (67). ASIT seawater analysis with Flowcam can be found at https://doi.org/10.6096/4007 (77) and Flow Cytometry data at https://doi.org/10.6096/4008 (76). Baring Head API-ToF data can be downloaded at https://doi.org/10.6096/4001 (87), PSM data can be accessed at https://doi.org/10.25326/355 (85) and CPC data at https://doi.org/10.25326/354 (86). The API-ToF data from Maido used to create Fig. 2 are available at https://doi.org/10.5281/zenodo.10022626 (79).

ACKNOWLEDGMENTS. The Sea2Cloud project is endorsed by SOLAS. We acknowledge the support and expertise of the Officers and Crew of the R/V Tangaroa and National Institute of Water and Atmospheric Research (NIWA) Vessel Services. This research received funding from the European Research Council (ERC) under the Horizon 2020 research and innovation program (Sea2Cloud grant agreement number - 771369 and grant agreement number 101002728) and was supported by NIWA SSIF funding to the Ocean-Climate Interactions, and Flows and Productivity Programs. The support from the Academy of Finland (331207) and the German Academic Exchange Service (DAAD) is greatly appreciated.

Author affiliations: [a]Université Clermont Auvergne, CNRS, Laboratoire de Météorologie Physique, Clermont-Ferrand F-63000, France; [b]Aerosol Physics Laboratory, Faculty of Engineering and Natural Sciences, University of Tampere, Tampere 33720, Finland; [c]Chemistry Department, Molecular Research Unit, University of Helsinki, Helsinki 00014, Finland; [d]Research Center for Marine Geosciences, Helmholtz Centre for Ocean Research Kiel, Kiel 24105, Germany; [e]Department of Atmospheric Chemistry and Climate, Institute of Physical Chemistry Blas Cabrera, Consejo Superior de Investigaciones Científicas, Madrid 28006, Spain; [f]National Institute of Water and Atmospheric Research, Wellington 6021, New Zealand; [g]Department of Marine Sciences, University of Otago, Dunedin 9016, New Zealand; [h]National Institute of Water and Atmospheric Research, Hamilton 3216, New Zealand; and [i]Commonwealth Scientific and Industrial Research Organisation Environment, Aspendale VIC 3195, Australia

1. S. Twomey, The influence of pollution on the shortwave albedo of clouds. *J. Atmos. Sci.* **34**, 1149–1152 (1977).
2. B. A. Albrecht, Aerosols, cloud microphysics, and fractional cloudiness. *Science* **245**, 1227–1230 (1989).
3. R. J. Charlson, J. E. Lovelock, M. O. Andreae, S. G. Warren, Oceanic phytoplankton, atmospheric sulphur, cloud albedo and climate. *Nature* **326**, 655–661 (1987).
4. T. Jokinen *et al.*, Ion-induced sulfuric acid–ammonia nucleation drives particle formation in coastal Antarctica. *Sci. Adv.* **4**, eaat9744 (2018).
5. L. J. Beck *et al.*, Differing mechanisms of new particle formation at two arctic sites. *Geophys. Res. Lett.* **48**, e2020GL091334 (2021).
6. A. Baccarini *et al.*, Low-volatility vapors and new particle formation over the southern ocean during the Antarctic circumnavigation expedition. *J. Geophys. Res. Atmos.* **126**, e2021JD035126 (2021).
7. J. Brean *et al.*, Open ocean and coastal new particle formation from sulfuric acid and amines around the Antarctic Peninsula. *Nat. Geosci.* **14**, 383–388 (2021).
8. C. D. O'Dowd *et al.*, Marine aerosol formation from biogenic iodine emissions. *Nature* **417**, 632–636 (2002).
9. M. Sipilä *et al.*, Molecular-scale evidence of aerosol particle formation via sequential addition of HIO3. *Nature* **537**, 532–534 (2016).
10. A. Baccarini *et al.*, Frequent new particle formation over the high Arctic pack ice by enhanced iodine emissions. *Nat. Commun.* **11**, 4924 (2020).
11. M. Peltola *et al.*, New particle formation in coastal New Zealand with a focus on open-ocean air masses. *Atmos. Chem. Phys.* **22**, 6231–6254 (2022).
12. C. O'Dowd, C. Monahan, M. Dall'Osto, On the occurrence of open ocean particle production and growth events: Marine particle production and growth. *Geophys. Res. Lett.* **37**, L19805 (2010).
13. K. Sellegri *et al.*, Sea2Cloud: From biogenic emission fluxes to cloud properties in the South West Pacific. *Bull. Am. Meteorol. Soc.* **104**, E1017–E1043 (2023), 10.1175/BAMS-D-21-0063.1 (17 April 2023).
14. O. R. Cooper *et al.*, Multi-decadal surface ozone trends at globally distributed remote locations. *Elem. Sci. Anthr.* **8**, 23 (2020).
15. V.-M. Kerminen, Atmospheric new particle formation and growth: Review of field observations. *Environ. Res. Lett.* **39**, 103003 (2018).
16. C. Zhang, X. Cao, X. Sun, H. Peng, Study on the formation of secondary organic aerosol by ozonolysis of citral in the atmosphere. *Aerosol Air Qual. Res.* **21**, 200637 (2021).
17. Y. Guo *et al.*, Formation of nighttime sulfuric acid from the ozonolysis of alkenes in Beijing. *Atmos. Chem. Phys.* **21**, 5499–5511 (2021).
18. P. R. Veres *et al.*, Global airborne sampling reveals a previously unobserved dimethyl sulfide oxidation mechanism in the marine atmosphere. *Proc. Natl. Acad. Sci. U.S.A.* **117**, 4505–4510 (2020).
19. G. A. Novak *et al.*, Rapid cloud removal of dimethyl sulfide oxidation products limits SO_2 and cloud condensation nuclei production in the marine atmosphere. *Proc. Natl. Acad. Sci. U.S.A.* **118**, e2110472118 (2021).
20. J. Shen *et al.*, High gas-phase methanesulfonic acid production in the OH-initiated oxidation of dimethyl sulfide at low temperatures. *Environ. Sci. Technol.* **56**, 13931–13944 (2022).
21. C. Rose *et al.*, Observations of biogenic ion-induced cluster formation in the atmosphere. *Sci. Adv.* **4**, eaar5218 (2018).
22. R. Talbot *et al.*, Tropospheric reactive odd nitrogen over the South Pacific in austral springtime. *J. Geophys. Res.* **105**, 6681–6694 (2000).
23. M. Kulmala *et al.*, Direct observations of atmospheric aerosol nucleation. *Science* **339**, 943–946 (2013).
24. S. M. Murphy *et al.*, Secondary aerosol formation from atmospheric reactions of aliphatic amines. *Atmos. Chem. Phys.* **7**, 2313–2337 (2007).
25. A. Kürten, New particle formation from sulfuric acid and ammonia: Nucleation and growth model based on thermodynamics derived from CLOUD measurements for a wide range of conditions. *Atmos. Chem. Phys.* **19**, 5033–5050 (2019).

Downloaded from https://www.pnas.org by CSIC UNIDAD DE RECURSOS DE INFORMAC on January 26, 2024 from IP address 161.111.20.207.

26. S. Chee, N. Myllys, K. C. Barsanti, B. M. Wong, J. N. Smith, An experimental and modeling study of nanoparticle formation and growth from dimethylamine and nitric acid. *J. Phys. Chem. A* **123**, 5640–5648 (2019).
27. M. Wang *et al.*, Synergistic HNO3–H2SO4–NH3 upper tropospheric particle formation. *Nature* **605**, 483–489 (2022).
28. J. H. Seinfeld, S. N. Pandis, *Atmospheric Chemistry and Physics: From Air Pollution to Climate Change* (Wiley, ed. 3, 2016).
29. J. Kirkby *et al.*, Role of sulphuric acid, ammonia and galactic cosmic rays in atmospheric aerosol nucleation. *Nature* **476**, 429–433 (2011).
30. J. Almeida *et al.*, Molecular understanding of sulphuric acid–amine particle nucleation in the atmosphere. *Nature* **502**, 359–363 (2013).
31. J. Kirkby *et al.*, Ion-induced nucleation of pure biogenic particles. *Nature* **533**, 521–526 (2016).
32. X.-C. He *et al.*, Role of iodine oxoacids in atmospheric aerosol nucleation. *Science* **371**, 589–595 (2021).
33. F. L. Eisele, Natural and anthropogenic negative ions in the troposphere. *J. Geophys. Res.* **94**, 2183 (1989).
34. M. Ehn *et al.*, A large source of low-volatility secondary organic aerosol. *Nature* **506**, 476–479 (2014).
35. L. J. Beck *et al.*, Diurnal evolution of negative atmospheric ions above the boreal forest: From ground level to the free troposphere. *Atmos. Chem. Phys.* **22**, 8547–8577 (2022).
36. F. Bianchi *et al.*, The role of highly oxygenated molecules (HOMs) in determining the composition of ambient ions in the boreal forest. *Atmos. Chem. Phys.* **17**, 13819–13831 (2017).
37. F. Heintz, U. Platt, H. Flentje, R. Dubois, Long-term observation of nitrate radicals at the Tor Station, Kap Arkona (Rügen). *J. Geophys. Res. Atmos.* **101**, 22891–22910 (1996).
38. M. Rocco *et al.* "Air-Sea fluxes of dimethyl sulphide and methanethiol in the South-West Pacific" Gases/Field Measurements/Troposphere/Chemistry (chemical composition and reactions) (2023), 10.5194/egusphere-2023-516 (10 July 2023).
39. M. Peltola *et al.*, Chemical precursors of new particle formation in coastal New Zealand. *Atmos. Chem. Phys.* **23**, 3955–3983 (2023).
40. R. Sander, Compilation of Henry's law constants (version 4.0) for water as solvent. *Atmos. Chem. Phys.* **15**, 4399–4981 (2015).
41. Y. Tian *et al.*, Nitric oxide (NO) in the Bohai Sea and the Yellow Sea. *Biogeosciences* **16**, 4485–4496 (2019).
42. B. M. Schieler *et al.*, Nitric oxide production and antioxidant function during viral infection of the coccolithophore Emiliania huxleyi. *ISME J.* **13**, 1019–1031 (2019).
43. W. Sunda, D. J. Kieber, R. P. Kiene, S. Huntsman, An antioxidant function for DMSP and DMS in marine algae. *Nature* **418**, 317–320 (2002).
44. Z. Zhang *et al.*, Discovery of nitric oxide in marine ecological system and the chemical characteristics of nitric oxide. *Sci. China Ser. B Chem.* **49**, 475–480 (2006).
45. C. Liu *et al.*, Evidence for the mutual effects of dimethylsulfoniopropionate and nitric oxide during the growth of marine microalgae. *Nitric Oxide* **42**, 54–61 (2014).
46. K. D. Bidle, Programmed cell death in unicellular phytoplankton. *Curr. Biol.* **26**, R594–R607 (2016).
47. S. Becker *et al.*, Laminarin is a major molecule in the marine carbon cycle. *Proc. Natl. Acad. Sci. U.S.A.* **117**, 6599–6607 (2020).
48. M. A. Moran *et al.*, Deciphering ocean carbon in a changing world. *Proc. Natl. Acad. Sci. U.S.A.* **113**, 3143–3151 (2016).
49. M. J. Kim *et al.*, Bacteria-driven production of alkyl nitrates in seawater: Bacterial production of alkyl nitrates. *Geophys. Res. Lett.* **42**, 597–604 (2015).
50. F. Schreiber, P. Wunderlin, K. M. Udert, G. F. Wells, Nitric oxide and nitrous oxide turnover in natural and engineered microbial communities: Biological pathways, chemical reactions, and novel technologies. *Front. Microbiol.* **3**, 372 (2012).
51. A. Abada *et al.*, Aerobic bacteria produce nitric oxide via denitrification and promote algal population collapse. *ISME J.* **17**, 1167–1183 (2023), 10.1038/s41396-023-01427-8 (18 July 2023).
52. J. D. Caranto, K. M. Lancaster, Nitric oxide is an obligate bacterial nitrification intermediate produced by hydroxylamine oxidoreductase. *Proc. Natl. Acad. Sci. U.S.A.* **114**, 8217–8222 (2017).
53. M. M. M. Kuypers, H. K. Marchant, B. Kartal, The microbial nitrogen-cycling network. *Nat. Rev. Microbiol.* **16**, 263–276 (2018).
54. F. Schreiber, P. Stief, M. M. M. Kuypers, D. de Beer, Nitric oxide turnover in permeable river sediment. *Limnol. Oceanogr.* **59**, 1310–1320 (2014).
55. X. S. Wan *et al.*, Phytoplankton-nitrifier interactions control the geographic distribution of nitrite in the upper ocean. *Glob. Biogeochem. Cycles* **35**, e2021GB007072 (2021).
56. A. M. N. Caruana, G. Malin, The variability in DMSP content and DMSP lyase activity in marine dinoflagellates. *Prog. Oceanogr.* **120**, 410–424 (2014).
57. G. V. Wolfe, B. F. Sherr, "Release and consumption of DMSP from Emiliania huxleyi during grazing by Oxyrrhis marina". *Mar. Ecol. Prog. Ser.* **111**, 111–119 (1994).
58. K. E. Altieri, S. E. Fawcett, M. G. Hastings, Reactive nitrogen cycling in the atmosphere and ocean. *Annu. Rev. Earth Planet. Sci.* **49**, 523–550 (2021).
59. T. Dobashi *et al.*, Marine nitrogen fixation as a possible source of atmospheric water-soluble organic nitrogen aerosols in the subtropical North Pacific. *Biogeosciences* **20**, 439–449 (2023).
60. T. E. G. Biggs, J. Huisman, C. P. D. Brussaard, Viral lysis modifies seasonal phytoplankton dynamics and carbon flow in the Southern Ocean. *ISME J.* **15**, 3615–3622 (2021).
61. E. Horas, L. Theodosiou, L. Becks, Why are algal viruses not always successful? *Viruses* **10**, 474 (2018).
62. M. P. Rissanen *et al.*, $CH_2NH_2 + O_2$ and $CH_3\,CHNH_2 + O_2$ Reaction kinetics: Photoionization mass spectrometry experiments and master equation calculations. *J. Phys. Chem. A* **118**, 2176–2186 (2014).
63. H. Gordon *et al.*, Causes and importance of new particle formation in the present-day and preindustrial atmospheres: Causes and role of new particle formation. *J. Geophys. Res. Atmos.* **122**, 8739–8760 (2017).
64. M. Peltola, G. Chamba, K. Sellegri, Sea2Cloud - Tangaroa - ASIT - PSM - Level 0. [Dataset]. Dataterra. https://doi.org/10.6096/4009. Accessed 3 November 2023.
65. M. Peltola, K. Sellegri, Sea2Cloud - Tangaroa - ASIT - CPC - Level 0. [Dataset]. Dataterra. https://doi.org/10.6096/4011. Accessed 3 November 2023.
66. M. Rocco, M. Peltola, K. Sellegri, Sea2Cloud - Tangaroa - ASIT - Ozone analyzer - Level 0. [Dataset]. Dataterra. https://doi.org/10.6096/4013. Accessed 3 November 2023.
67. M. Rocco, M. Peltola, K. Sellegri, Sea2Cloud - Tangaroa - ASIT - SO2 analyzer - Level 0. [Dataset]. Dataterra. https://doi.org/10.6096/4012. Accessed 3 November 2023.
68. M. Rocco, E. Dunne, K. Sellegri, Sea2Cloud - Tangaroa - ASIT - PTRMS - Level 1. [Dataset]. Dataterra. https://doi.org/10.6096/4010. Accessed 3 November 2023.
69. M. Rocco *et al.*, Oceanic phytoplankton are a potentially important source of benzenoids to the remote marine atmosphere. *Commun. Earth Environ.* **2**, 175 (2021).
70. M. Peltola, G. Chamba, K. Sellegri, Sea2Cloud - Tangaroa - ASIT - CIAPIToF - Level 1. [Dataset]. Dataterra. https://doi.org/10.6096/4014. Accessed 3 November 2023.
71. T. Jokinen *et al.*, Atmospheric sulphuric acid and neutral cluster measurements using CI-APi-TOF. *Atmos. Chem. Phys.* **12**, 4117–4125 (2012).
72. M. Peltola, G. Chamba, K. Sellegri, Sea2Cloud - Tangaroa - ASIT - APIToF - Level 1. [Dataset]. Dataterra. https://doi.org/10.6096/4015. Accessed 3 November 2023.
73. H. Junninen *et al.*, A high-resolution mass spectrometer to measure atmospheric ion composition. *Atmos. Meas. Tech.* **3**, 1039–1053 (2010).
74. K. Willeke, P. A. Baron, *Aerosol Measurement: Principles, Techniques, and Applications* (Van Nostrand Reinhold, 1993).
75. L. J. Beck, S. Schobesberger, M. Sipilä, V.-M. Kerminen, M. Kulmala, Estimation of sulfuric acid concentration using ambient ion composition and concentration data obtained with atmospheric pressure interface time-of-flight ion mass spectrometer. *Atmos. Meas. Tech.* **15**, 1957–1965 (2022).
76. S. Deppeler, C. Law, Sea2Cloud - Tangaroa - ASIT - Flow Cytometry - Level 2. [Dataset]. Dataterra. https://doi.org/10.6096/4008. Accessed 3 November 2023.
77. K. Safi, C. Law, Sea2Cloud - Tangaroa - ASIT - Flowcam - Level 2. [Dataset]. Dataterra. https://doi.org/10.6096/4007. Accessed 3 November 2023.
78. S. Mirme, A. Mirme, The mathematical principles and design of the NAIS–A spectrometer for the measurement of cluster ion and nanometer aerosol size distributions. *Atmos. Meas. Tech.* **6**, 1061–1071 (2013).
79. G. Chamba, S. Iyer, C. Rose, K. Sellegri, M. Rissanen, Data presented in figure 2 of "Evidence of nitrate based nighttime atmospheric nucleation driven by marine microorganisms in the South Pacific" [Data set]. Zenodo. https://doi.org/10.5281/zenodo.10022626. Accessed 15 October 2023.
80. C. Rose *et al.*, CCN production by new particle formation in the free troposphere. *Atmos. Chem. Phys.* **17**, 1529–1541 (2017).
81. H. Venzac, K. Sellegri, P. Villani, D. Picard, P. Laj, Seasonal variation of aerosol size distributions in the free troposphere and residual layer at the puy de Dôme station, France. *Atmos. Chem. Phys.* **9**, 1465–1478 (2009).
82. A. Farah *et al.*, Seasonal variation of aerosol size distribution data at the puy de Dôme station with emphasis on the boundary layer/free troposphere segregation. *Atmosphere* **9**, 244 (2018).
83. B. Foucart *et al.*, High occurrence of new particle formation events at the Maïdo high-altitude observatory (2150 m), Réunion (Indian Ocean). *Atmos. Chem. Phys.* **18**, 9243–9261 (2018).
84. C. Rose *et al.*, New particle formation in the volcanic eruption plume of the Piton de la Fournaise: Specific features from a long-term dataset. *Atmos. Chem. Phys.* **19**, 13243–13265 (2019).
85. M. Peltola, M. Harvey, K. Sellegri, Sea2Cloud - Baring-Head - PSM - Level 2. [Dataset]. Dataterra. https://doi.org/10.25326/355. Accessed 3 November 2022.
86. M. Peltola, M. Harvey, K. Sellegri, Sea2Cloud - Baring-Head - CPC - Level 0. [Dataset]. Dataterra. https://doi.org/10.25326/354. Accessed 1 December 2022.
87. M. Peltola, M. Harvey, K. Sellegri, Sea2Cloud - Baring-Head - APi-TOF - Level 2. [Dataset]. Dataterra. https://doi.org/10.6096/4001. Accessed 1 December 2022.
88. J. Zhang, M. Dolg, Global optimization of clusters of rigid molecules using the artificial bee colony algorithm. *Phys. Chem. Chem. Phys.* **18**, 3003–3010 (2016).
89. J. Kubečka, V. Besel, T. Kurtén, N. Myllys, H. Vehkamäki, Configurational sampling of noncovalent (atmospheric) molecular clusters: Sulfuric acid and guanidine. *J. Phys. Chem. A* **123**, 6022–6033 (2019).
90. K. Vanommeslaeghe *et al.*, CHARMM general force field: A force field for drug-like molecules compatible with the CHARMM all-atom additive biological force fields. *J. Comput. Chem.* **31**, 671–690 (2009).
91. F. Neese, F. Wennmohs, U. Becker, C. Riplinger, The ORCA quantum chemistry program package. *J. Chem. Phys.* **152**, 224108 (2020).

Downloaded from https://www.pnas.org by CSIC UNIDAD DE RECURSOS DE INFORMAC on January 26, 2024 from IP address 161.111.20.207.